

Inverse conductivity problem with an imperfectly known boundary

Ville Kolehmainen*, Matti Lassas† and Petri Ola‡

Abstract. We show how to eliminate the error caused by an incorrectly modeled boundary in electrical impedance tomography (EIT). In practical measurements, one usually lacks the exact knowledge of the boundary. Because of this the numerical reconstruction from the measured EIT-data is done using a model domain that represents the best guess for the true domain. However, it has been noticed that the inaccurate model of the boundary causes severe errors for the reconstructions. We introduce a new algorithm to find a deformed image of the original isotropic conductivity based on the theory of Teichmüller spaces and implement it numerically.

AMS classification: 35J25, 30C75.

Keywords: Inverse conductivity problem, electrical impedance tomography, unknown boundary, Teichmüller mapping.

1. Introduction. We consider the electrical impedance tomography (EIT) problem, i.e. the determination of an unknown conductivity distribution inside a domain, for example the human thorax, from voltage and current measurements made on the boundary. Mathematically this is formulated as follows: Let $\Omega \subset \mathbb{R}^2$ be the measurement domain, and denote by $\gamma = (\gamma^{ij})$ the symmetric matrix describing the conductivity in Ω . We assume that the matrix has components in $L^\infty(\Omega)$ and that it is strictly positive definite, that is, for some $c > 0$ we have $\langle \xi, \gamma(x)\xi \rangle \geq c\|\xi\|^2$ for all $x \in \Omega$. The electrical potential u satisfies in Ω the equation

$$(1.1) \quad \nabla \cdot \gamma \nabla u = 0.$$

To uniquely fix the solution u it is enough to give its value on the boundary. Let this be $u|_{\partial\Omega} = f \in H^{1/2}(\partial\Omega)$ where $H^{1/2}(\partial\Omega)$ is the Sobolev space. Then (1.1) has a unique weak solution $u \in H^1(\Omega)$.

Our boundary data is the map that takes the voltage distribution f on the boundary for all f to the corresponding current flux through the boundary, $\nu \cdot \gamma \nabla u$, where ν is the exterior unit normal to Ω . Mathematically this amounts to the knowledge of the Dirichlet–Neumann map Λ corresponding to γ , i.e. the map taking the Dirichlet boundary values to

*University of Kuopio, Department of Applied Physics, P.O.Box 1627, FIN-70211 Finland

†Helsinki University of Technology, Institute of Mathematics, P.O.Box 1100, FIN-02015, Finland

‡Rolf Nevanlinna Institute, University of Helsinki Helsinki, P.O.Box 4, FIN-00014, Finland

the corresponding Neumann boundary values of the solution to (1.1),

$$\Lambda_\gamma : u|_{\partial\Omega} \mapsto \sum_{i,j=1}^2 \nu_i \gamma^{ij} \frac{\partial u}{\partial x_j} \Big|_{\partial\Omega}.$$

This defines a bounded operator $\Lambda_\gamma : H^{1/2}(\partial\Omega) \rightarrow H^{-1/2}(\partial\Omega)$. The symmetric quadratic form corresponding to Λ_γ ,

$$(1.2) \quad \Lambda_\gamma[h, h] := \int_{\partial\Omega} h \Lambda_\gamma h \, dS = \int_{\partial\Omega} \nabla u \cdot \gamma \nabla u \, dx$$

equals in physical terms the power needed to maintain the potential h on $\partial\Omega$.

When γ is a scalar valued function times identity matrix, we say that the conductivity is *isotropic*. As usual, conductivities that may be matrix-valued are referred as *anisotropic* conductivities. The EIT–problem is to reconstruct γ from Λ_γ . The problem was originally proposed by Calderón [6] and then solved in dimensions three and higher for isotropic smooth conductivities in [18]. The two dimensional case that is relevant to us was solved by Nachman [13] for isotropic conductivities assuming $\gamma \in W^{2,p}$, $p > 1$ and then finally for general L^∞ –smooth isotropic conductivities by Astala and Päiväranta in a celebrated paper [4].

The conductivity equation is invariant under deformations of the domain Ω in the following sense. If F is a diffeomorphism taking Ω to some other domain $\tilde{\Omega}$, then $u \circ F^{-1}$ will satisfy the conductivity equation in $\tilde{\Omega}$ with conductivity

$$(1.3) \quad \tilde{\gamma}(x) = \frac{F'(y) \gamma(y) (F'(y))^t}{|\det F'(y)|} \Big|_{y=F^{-1}(x)},$$

where F' is the Jacobi matrix of map F and u is a solution of $\nabla \cdot \gamma \nabla u = 0$ in Ω . We say that $\tilde{\gamma}$ is the push forward of γ by F and denote it by $\tilde{\gamma} = F_*\gamma$. Note that all this is well defined for general matrix valued γ . For us the starting point is the trivial observation that even if γ is isotropic, the deformed conductivity $\tilde{\gamma}$ will not in general be isotropic. The boundary measurements are invariant: When $f : \partial\Omega \rightarrow \partial\tilde{\Omega}$ is the restriction of $F : \Omega \rightarrow \tilde{\Omega}$, we say that $\tilde{\Lambda} = f_*\Lambda_\gamma$,

$$((f_*\Lambda_\gamma)h)(x) = (\Lambda_\gamma(h \circ f))(y)|_{y=f^{-1}(x)}, \quad h \in H^{1/2}(\partial\tilde{\Omega})$$

is the push forward of Λ_γ in f . As seen in [17], it turns out that $f_*\Lambda_\gamma = \Lambda_{F_*\gamma}$.

The facts that the anisotropic conductivity equation and the boundary measurements are invariant has the important consequence that the EIT–problem with an anisotropic conductivity is not uniquely solvable, even though the isotropic problem is, see [17].

In practice when solving the EIT–problem in a given domain Ω , one typically seeks for the isotropic conductivity that minimizes

$$(1.4) \quad \|\Lambda_{meas} - \Lambda_\gamma\|^2 + \alpha \|\gamma\|_X^2$$

for γ defined in terms of some triangulation of Ω as e.g. a piecewise constant function and $\|\cdot\|_X$ is some regularization norm [10]. Here Λ_{meas} is the measurement of the Dirichlet–Neumann map that contains measurement errors.

In practice, one of the key difficulties in solving the EIT problem is that the domain Ω may not be known accurately. It has been noticed that the use of slightly incorrect model for Ω , i.e., a slightly incorrect model of the boundary causes serious errors in reconstructions, see e.g. [9, 1, 8]. As an example, consider the EIT measurements of pulmonary function from the human thorax. The measurement electrodes are attached on the skin of the patient around the thorax. In principle, an exact parameterization for the shape of the thorax could be obtained from other medical imaging modalities such as magnetic resonance imaging (MRI) or computerized tomography (CT). However, in most cases these data is not available, and one has to resort to some approximate thorax model. Further, the shape of the thorax varies between breathing states, and it is also dependent on the orientation of the patient. Thus, the thorax geometry is known inaccurately even in the best case scenarios.

In this paper our aim is to propose a method to overcome the problem that the boundary and its parameterization are not exactly known. The set-up of the problem we consider is the following:

We want to recover the unknown conductivity γ in Ω from the measurements of Dirichlet-to-Neumann map, and we assume a priori that γ is isotropic. We assume $\partial\Omega$ and Λ_γ are not known. Instead, let Ω_m , called the model domain, be our best guess for the domain and let $f_m : \partial\Omega \rightarrow \partial\Omega_m$ be a diffeomorphism modeling the approximate knowledge of the boundary. As the data for the inverse problem, we assume that we are given the boundary of the model domain, $\partial\Omega_m$ and the map $\Lambda_m := (f_m)_* \Lambda_\gamma$ on $\partial\Omega_m$. Note that we have simplified the problem by assuming that the only error in Λ_m comes from the imperfect knowledge of the boundary.

This set-up is motivated by the fact that the quadratic form corresponding to Λ_m ,

$$\Lambda_m[h, h] = \int_{\partial\Omega_m} h \Lambda_m h \, dS = \int_{\partial\Omega} (h \circ f_m) \Lambda_\gamma (h \circ f_m) \, dS, \quad h \in H^{1/2}(\partial\Omega_m)$$

equals physically to the power needed to maintain the potential $h \circ f_m$ on $\partial\Omega$.

Since Λ_m usually does not correspond to any isotropic conductivity because of the deformation done when going from the original domain Ω to Ω_m , we obtain an erroneous solution γ when solving the minimization problem (1.4). This means that a systematic error in domain model causes a systematic error to the reconstruction. In particular, local changes of the conductivity often give raise to non-localized changes in reconstructions due to the above systematic error. Thus the spatial resolution of details of reconstructions are often weak. This is clearly seen in practical measurements, see e.g. [8].

We note that one could forget in solving of the minimization problem (1.4) the assumption that γ is isotropic, and find the minimizer in the set of anisotropic conductivities. However, the anisotropic inverse problem has non-unique solution, and as the minimization problem is highly non-convex, the minimization would be hard and, as usual, forgetting existing a priori information makes the solution significantly worse.

To formulate our main results, let us define certain concepts. We start with the maximal anisotropy of an anisotropic conductivity.

DEFINITION 1.1. *Let $\gamma^{jk}(x)$ be an $L^\infty(\Omega)$ -smooth matrix valued conductivity in Ω and let $\lambda_1(x)$ and $\lambda_2(x)$, $\lambda_1(x) \geq \lambda_2(x)$ be the eigenvalues of matrix $\gamma^{jk}(x)$. We define the maximal*

anisotropy of a conductivity to be $K(\gamma)$ given by

$$K(\gamma) = \sup_{x \in \Omega} K(\gamma, x), \quad \text{where } K(\gamma, x) = \frac{\sqrt{L(x)} - 1}{\sqrt{L(x)} + 1}, \quad L(x) = \frac{\lambda_1(x)}{\lambda_2(x)}.$$

We call the function $K(\gamma, x)$ the anisotropy of γ at x . Here \sup denotes the essential supremum.

Sometimes, to indicate the domain Ω , we denote $K(\gamma) = K_\Omega(\gamma)$. As a particularly important example needed later, let us consider the conductivity matrices of the form

$$(1.5) \quad \widehat{\gamma}(x) = \eta(x) R_{\theta(x)} \begin{pmatrix} \lambda^{1/2} & 0 \\ 0 & \lambda^{-1/2} \end{pmatrix} R_{\theta(x)}^{-1}$$

where $\lambda \geq 1$ is a constant, $\eta(x) \in \mathbb{R}_+$ is a real valued function, $R_{\theta(x)}$ is a rotation matrix corresponding to angle $\theta(x)$, where

$$R_\theta = \begin{pmatrix} \cos \theta & \sin \theta \\ -\sin \theta & \cos \theta \end{pmatrix}.$$

We denote such conductivities by $\widehat{\gamma} = \widehat{\gamma}_{\lambda, \theta, \eta}$. These conductivities have the anisotropy $K(\widehat{\gamma}, x) = c_\lambda = (\lambda^{1/2} - 1)/(\lambda^{1/2} + 1)$ at every point and thus their maximal anisotropy is $K = c_\lambda$. We call such conductivities $\widehat{\gamma}$ *uniformly anisotropic conductivities*.

The following theorem is the main result of the paper.

THEOREM 1.2. *Let Ω be a bounded, simply connected $C^{1,\alpha}$ -domain with $\alpha > 0$. Assume that $\gamma \in C^{0,\alpha}(\overline{\Omega})$ is an isotropic conductivity and Λ_γ its Dirichlet–Neumann map. Let Ω_m be a model of the domain (which is assumed to satisfy the same regularity assumptions as Ω), and $f_m : \partial\Omega \rightarrow \partial\Omega_m$ be a $C^{1,\alpha}$ -smooth diffeomorphism.*

Assume that we are given $\partial\Omega_m$ and $\Lambda_m = (f_m)_ \Lambda_\gamma$. Then*

1. *There are unique $\lambda \geq 1$, $\theta \in L^\infty(\Omega_m, S^1)$ and $\eta \in L^\infty(\Omega_m, \mathbb{R}_+)$ such that the conductivity $\widehat{\gamma} = \widehat{\gamma}_{\lambda, \theta, \eta}$ satisfies $\Lambda_{\widehat{\gamma}} = \Lambda_m$.*
2. *If γ_2 is an anisotropic conductivity in Ω_m such that $\Lambda_{\gamma_2} = \Lambda_m$ then $K(\gamma_2) \geq K(\widehat{\gamma})$. Moreover, $K(\gamma_2) = K(\widehat{\gamma})$ if and only if $\gamma_2 = \widehat{\gamma}$.*

Theorem 1.2 can be interpreted by saying that we can find a unique conductivity in Ω_m that is as close as possible to being isotropic.

The proof of Theorem 1.2 is based on the theory of quasiconformal maps. There are several equivalent definitions for these maps, and we will present the one based on a partial differential equation (Beltrami equation) in Section 2. However, the quasiconformal maps have also a geometric definition. Indeed, they are generalizations of conformal maps that take infinitesimal disks at z to infinitesimal disks at $f(z)$, and the radii gets dilated by $|f'(z)|$. Analogously, a homeomorphic map is quasiconformal on a domain Ω if infinitesimal disks at any $z \in \Omega$ get mapped to infinitesimal ellipsoids at $f(z)$. The ratio of the larger semiaxis to smaller semiaxis is called the dilation of f at z , and the supremum of dilatations over Ω is the maximal dilation. This dilatation of infinitesimal discs is in fact the reason why

isotropic conductivities change to anisotropic ones in push forwards with quasiconformal maps.

The crucial fact that we use proving Theorem 1.2 is a result of Strebel [16], that roughly speaking says that among all quasiconformal self-maps of the unit disk to itself with a given sufficiently smooth boundary value there is a unique one with the minimal maximal dilation. This will yield that corresponding to the given boundary modeling map $f_m : \partial\Omega \rightarrow \partial\Omega_m$ there is a unique map $F : \Omega \rightarrow \Omega_m$ having the minimal maximal dilation. We will show that this leads to the following result:

PROPOSITION 1.3. *Let Ω , γ , Ω_m , and f_m satisfy assumptions of Theorem 1.2. Then there is a unique map $F : \Omega \rightarrow \Omega_m$, depending only on $f : \partial\Omega \rightarrow \partial\Omega_m$ such that for the uniformly anisotropic conductivity $\hat{\gamma}$ corresponding to γ in Theorem 1.2 we have*

$$(1.6) \quad \det(\hat{\gamma}(x))^{1/2} = \gamma(F^{-1}(x)).$$

Proposition 1.3 can be interpreted as saying that solving the minimization problem (1.4) with $\alpha = 0$ in the class of conductivities $\hat{\gamma}_{\lambda,\theta,\eta}$ we can find the function $(\det \hat{\gamma}(x))^{1/2}$ in Ω_m that represents a deformed image of original conductivity γ in the unknown domain Ω and the deformation depends only on the error made in modeling the boundary, not on the conductivity in Ω .

In particular, this turns out to be useful as local perturbations of conductivity remain local in reconstruction: if we consider one fixed boundary modeling map $f_m : \partial\Omega \rightarrow \partial\Omega_m$ but two isotropic conductivities γ_1 and $\gamma_2 = \gamma_1 + \sigma$ in Ω , then the reconstructions $\hat{\gamma}_1$ and $\hat{\gamma}_2$ obtained by Theorem 1.2 corresponding to γ_1 and γ_2 satisfy

$$\det(\hat{\gamma}_2(x))^{1/2} - \det(\hat{\gamma}_1(x))^{1/2} = \sigma(F^{-1}(x)).$$

Remark 1. Theorem 1.2 holds for anisotropic conductivities in the sense that for each $C^{1,\alpha}(\bar{\Omega})$ -smooth anisotropic conductivity γ there is a unique conductivity $\hat{\gamma} = \hat{\gamma}_{\lambda,\theta,\eta}$ such that $(f_m)_*\Lambda_\gamma = \Lambda_{\hat{\gamma}}$. However, for anisotropic conductivities Proposition 1.3 does not hold as the map F depends on the conformal class of γ .

The paper is organized as follows. In Section 2 we consider isotropization of anisotropic conductivity using a diffeomorphism and pay close attention to the smoothness required from γ and Ω and introduce the necessary background from the theory anisotropic inverse problems. We apply this in Section 3 in proving main results using the existence of a Teichmüller mapping. In Section 4 we consider physically realistic measurements, i.e., so-called complete electrode model. The numerical implementation for the complete electrode model is then described in the last sections.

2. Quasiconformal maps and solvability of inverse problem with anisotropic conductivity. It is a classical result that every Riemannian surface is locally conformal to a Euclidean plane: this corresponds to choosing the coordinate system to be *isothermal*. Similarly, every anisotropic conductivity matrix can be transformed to an isotropic conductivity. We identify the plane \mathbb{R}^2 with complex plane \mathbb{C} .

LEMMA 2.1. *Let Ω be a bounded, simply connected $C^{1,\alpha}$ -domain with $\alpha > 0$. Assume that $\gamma \in C^{0,\alpha}(\overline{\Omega})$ is an isotropic conductivity. Then there is a $C^{1,\alpha}$ -smooth diffeomorphism $F : \overline{\Omega} \rightarrow \overline{\tilde{\Omega}}$, $\tilde{\Omega} = F(\Omega) \subset \mathbb{C}$ such that*

$$(2.7) \quad F_*\gamma = \beta,$$

where $F_*\gamma$ is defined by (1.3), and β is the identity matrix multiplied by a $C^{0,\alpha}$ -smooth scalar function. Moreover,

$$\beta = (\det \gamma \circ F^{-1})^{1/2} I.$$

The proof of this result is well known, but as smoothness of F is crucial later, we give the proof for the convenience of the reader.

Proof. The equation (2.7) a priori a nonlinear system for the derivatives of F . However, in two dimensions this equation completely linearizes, and is equivalent to the *Beltrami-equation*

$$(2.8) \quad \bar{\partial}F = \mu\partial F,$$

where the complex derivatives are $\partial = \frac{1}{2}(\frac{\partial}{\partial x} - i\frac{\partial}{\partial y})$, $\bar{\partial} = \frac{1}{2}(\frac{\partial}{\partial x} + i\frac{\partial}{\partial y})$ and the *Beltrami coefficient* $\mu = \mu_F(z)$, called also *complex dilatation* is given by

$$(2.9) \quad \mu = \frac{-\gamma_{11} + \gamma_{22} - 2i\gamma_{12}}{\gamma_{11} + \gamma_{22} + 2\sqrt{\gamma_{11}\gamma_{22} - \gamma_{12}^2}}.$$

The function μ has the crucial property that it is strictly less than one in modulus:

$$(2.10) \quad \sup_{z \in \Omega} |\mu(z)| < 1.$$

Let us extend the conductivity matrix γ (a priori only defined in Ω) to the whole plane to be the identity matrix outside Ω . Similarly, μ is extended outside Ω by zero.

Next we consider how to solve the Beltrami equation, and for this we consider it in the whole plane. In order to have a unique solution we fix the behaviour of F at infinity. Thus, consider

$$(2.11) \quad \begin{aligned} \bar{\partial}F(z) &= \mu(z)\partial F(z) \quad \text{in } \mathbb{C}, \\ F(z) &= z + h(z), \\ \lim_{z \rightarrow \infty} h(z) &= 0 \end{aligned}$$

where μ is a compactly supported L^∞ -function satisfying (2.10). This problem has unique solution $F \in L_\delta^p$ when p is close enough to 2 and $-2/p < \delta < 1 - 1/p$. For the proof of this see, for example [2] or [17]. The proof is based on the fact that (2.11) can be written as an integral equation

$$(2.12) \quad F(z) - \frac{1}{2\pi i} \int_{\mathbb{C}} \frac{\mu(\zeta)\partial F(\zeta)}{z - \zeta} da(\zeta) = z$$

where $da(\zeta)$ is Euclidean area in \mathbb{C} (or \mathbb{R}^2). As $\|\mu\|_\infty < 1$, it turns out that the left hand side of equation (2.12) is of the form of the identity plus a contractive operator in

Sobolev space $W^{1,p}(\Omega)$, with appropriate p , and thus equation (2.12) can be solved by an application of the Neumann–series argument.

Using interior Schauder estimates for equation (2.11), we see that if γ and thus μ are $C^{0,\alpha}$ –smooth, the solution F has to be locally $C^{1,\alpha}$ –smooth in \mathbb{C} , in particular in $\bar{\Omega}$. Using formula (1.3) we see that $F_*\gamma$ is $C^{0,\alpha}$ –smooth in closure of $\tilde{\Omega}$. \square .

In general, any solution $F : \Omega \rightarrow \tilde{\Omega}$ to Beltrami equation for μ satisfying (2.10) and for which $F \in H^1(\Omega)$ is called *quasiregular*. If a quasiregular map $F : \Omega \rightarrow \tilde{\Omega}$ is homeomorphism, it is said to be *quasiconformal*. The quasiconformality can be defined also in geometrical terms, see [2], [11].

Next we recall the recent results for inverse problems for anisotropic conductivities γ . Let us consider a class of conductivities in Ω , given by

$$\Sigma(\gamma) = \{F_*\gamma \mid F : \Omega \rightarrow \Omega \text{ is homeomorphism, } F, F^{-1} \in H^1(\Omega; \mathbb{C}), F|_{\partial\Omega} = I\},$$

that is, $\Sigma(\gamma)$ is the equivalence class of the conductivity γ in push forwards with boundary preserving diffeomorphisms. Then $\Lambda_\sigma = \Lambda_\gamma$ for all $\sigma \in \Sigma(\gamma)$. By [3], the converse is true, that is, if σ is a strictly positive definite L^∞ –conductivity and $\Lambda_\sigma = \Lambda_\gamma$, then $\sigma \in \Sigma(\gamma)$. In other words, Λ_γ determines the equivalence class $\Sigma(\gamma)$. Note that diffeomorphism $F : \Omega \rightarrow \Omega$ such that $F \in H^1(\Omega; \mathbb{C})$ and $F|_{\partial\Omega} = I$ is quasiconformal.

3. Proof of main results We start with the proof of Theorem 1.2. Note the fact that the conductivity γ in Ω is isotropic will not be used in the proof at all. First we show that we can assume that Ω_m is the unit disc $\mathbb{D} \subset \mathbb{C}$.

To prove this, let $f_m : \partial\Omega \rightarrow \partial\Omega_m$ be the boundary modeling map and γ a $C^{1,\alpha}$ –smooth (also possibly anisotropic) conductivity in $\bar{\Omega}$.

Our first observation is that as Ω_m is a simply connected domain, it follows from Riemann mapping theorem that it can be mapped to unit disc \mathbb{D} conformally. Moreover, as Ω_m is $C^{1,\alpha}$ –smooth domain it follows from Kellog–Warschawski theorem [14, Thm. 3.6], that the Riemann–map can be chosen to be a $C^{1,\alpha}$ –diffeomorphism $F_0 : \bar{\Omega}_m \rightarrow \bar{\mathbb{D}}$ such that $F_0 : \Omega_m \rightarrow \mathbb{D}$ is conformal. Thus, if σ is some $C^{0,\alpha}$ –smooth anisotropic conductivity in $\bar{\Omega}_m$, we have that $\sigma_0 = (F_0)_*\sigma$ is $C^{0,\alpha}(\bar{\mathbb{D}})$ –smooth conductivity.

Second, we observe that the uniformly anisotropic conductivity $\hat{\gamma}_{\lambda,\theta,\eta}$ of the form (1.5) in Ω_m changes under $(F_0)_*$ to a uniformly anisotropic conductivity $(F_0)_*\hat{\gamma}_{\lambda,\theta,\eta} = \hat{\gamma}_{\lambda,\theta_0,\eta_0}$ in \mathbb{D} such that $\eta_0 = \eta \circ F_0^{-1}$.

Third, we see that as $F_0 : \Omega_m \rightarrow \mathbb{D}$ is conformal, the maximal anisotropy of $(F_0)_*\sigma$ and σ satisfy

$$K_{\mathbb{D}}((F_0)_*\sigma) = K_{\Omega}(\sigma),$$

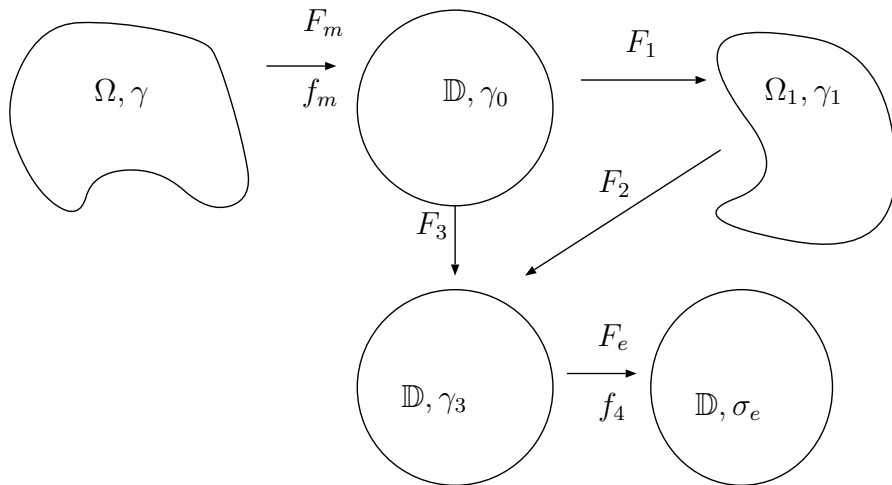
that is, the maximal anisotropy is preserved in conformal transformations for any σ .

Fourth, if $f_0 = F_0|_{\partial\Omega_m}$ then $\Lambda_{\sigma_0} = (f_0)_*\Lambda_\sigma$. Also, we see that the our data is invariant in the change of the model domain in the sense that $(\tilde{f}_m)_*\Lambda_\gamma = (f_0)_*((\tilde{f}_m)_*\Lambda_\gamma)$ where $\tilde{f}_m = f_0 \circ f_m : \partial\Omega \rightarrow \partial\mathbb{D}$.

These four observations yield that it is enough to prove the assertion in the case when $\Omega_m = \mathbb{D}$. Indeed, changing Ω_m to \mathbb{D} with F_0 keeps the boundary measurements, the smoothness of objects, the maximal anisotropy as well as class of uniformly anisotropic

conductivities invariant. More precisely, we can replace the boundary modeling map f_m by the map $\tilde{f}_m = f_0 \circ f_m$.

Thus, let us return proving Theorem 1.2 in the case when $\Omega_m = \mathbb{D}$. Let $f_m : \partial\Omega \rightarrow \partial\mathbb{D}$ be the boundary modeling map that is a $C^{1,\alpha}$ -smooth diffeomorphism and $\gamma \in C^{0,\alpha}(\overline{\Omega})$ be an isotropic conductivity with Dirichlet–Neumann map Λ_γ .



Let F_m be some $C^{1,\alpha}(\overline{\Omega})$ -diffeomorphism $F_m : \overline{\Omega} \rightarrow \overline{\mathbb{D}}$ such that $F_m|_{\partial\Omega} = f_m$. There are many ways to construct such map, and for convenience of the reader, we present one simple way. Let $G : \Omega \rightarrow \mathbb{D}$ be a Riemann-map. By [14, Thm. 3.7], G has $C^{1,\alpha}$ -extension $G : \overline{\Omega} \rightarrow \overline{\mathbb{D}}$. Let $\phi = f_m \circ G^{-1} : \partial\mathbb{D} \rightarrow \partial\mathbb{D}$ and $\Phi(z) = |z| \exp(i(|z|^3 \arg(\phi(z/|z|)) + (1-|z|^3) \arg(z/|z|)))$ be a $C^{1,\alpha}$ -diffeomorphism $\mathbb{D} \rightarrow \mathbb{D}$ satisfying $\Phi|_{\partial\mathbb{D}} = \phi$. Then F_m can be chosen to be the map $\Phi \circ G$.

Let $\gamma_0 = (F_m)_* \gamma$ be an anisotropic conductivity in \mathbb{D} . By Lemma 2.1, there is a $C^{1,\alpha}$ -diffeomorphism $F_1 : \overline{\Omega} \rightarrow \overline{\Omega}_1$ such that the conductivity $\gamma_1 = (F_1)_* \gamma_0$ is $C^{0,\alpha}$ -smooth isotropic conductivity in the closure of the $C^{1,\alpha}$ -smooth domain Ω_1 .

As Ω_1 is a simply connected $C^{1,\alpha}$ -smooth domain, by Kellog-Warschawski theorem cited above there is a conformal map $F_2 : \Omega_1 \rightarrow \mathbb{D}$ such that $F_2 : \overline{\Omega}_1 \rightarrow \overline{\mathbb{D}}$ is a $C^{1,\alpha}$ -diffeomorphism. Let $F_3 = F_2 \circ F_1 : \mathbb{D} \rightarrow \mathbb{D}$ and $f_3 = F_3|_{\partial\mathbb{D}}$. Note that $(F_3)_* \gamma_0$ is isotropic conductivity in \mathbb{D} as F_2 is conformal.

The boundary values of quasiconformal maps $\mathbb{D} \rightarrow \mathbb{D}$ are characterized as being the quasi-symmetric maps, that is, homeomorphic maps $f : \partial\mathbb{D} \rightarrow \partial\mathbb{D}$ such that $\theta(u) = \arg f(e^{iu})$ satisfy

$$(3.13) \quad k^{-1} \leq \frac{\theta(v) - \theta(u)}{\theta(v) - \theta(u)} \leq k, \quad \text{for all } u, v \in \partial\mathbb{D},$$

with some $k > 0$, see [11].

Let us consider next the map $f_4 = f_3^{-1} : \partial\mathbb{D} \rightarrow \partial\mathbb{D}$. Since f_3 and f_3^{-1} are $C^{1,\alpha}$ -smooth, we see that f_4 satisfies

$$(3.14) \quad \lim_{t \rightarrow 0} \frac{\theta(u+t) - \theta(u)}{\theta(u-t) - \theta(u)} = 1 \text{ uniformly in } u \in \partial\mathbb{D},$$

and is in particular quasi-symmetric. Thus f_4 is boundary value of at least one quasi-conformal map. What is more, since f_4 satisfies condition (3.14), it follows from results Strebel [16], that among all quasiconformal maps having f_4 as a boundary value there is a unique *extremal* map F_e in the sense that the L^∞ -norm of the complex dilatation μ_{F_e} is minimal. More precisely, if $F : \mathbb{D} \rightarrow \mathbb{D}$ is quasiconformal map such that $F|_{\partial\mathbb{D}} = f_4$, then its Beltrami coefficient satisfies $\|\mu_F\|_{L^\infty} \geq \|\mu_{F_e}\|_{L^\infty}$ and the equality holds only if $F = F_e$. Furthermore, the extremal F_e is a Teichmüller mapping, i.e., its complex dilatation μ_{F_e} is of the form

$$(3.15) \quad \mu_{F_e}(z) = \|\mu_{F_e}\|_{L^\infty} \frac{\overline{\phi(z)}}{|\phi(z)|},$$

where $\phi : \mathbb{D} \rightarrow \mathbb{C}$ is holomorphic in \mathbb{D} , and has thus discrete set of zeros. Note that as F_e need not to be even Lipschitz smooth near zeros of ϕ . Reader should also note that certain assumption on the regularity of the boundary value f_m is necessary for existence of extremal maps. This will be discussed after finishing the proof.

Let us now consider how a quasiconformal map $F : \mathbb{D} \rightarrow \mathbb{D}$ with complex dilatation μ_F change maximal anisotropy of conductivities. When σ is an isotropic conductivity in \mathbb{D} , that is, $K(\sigma) = 0$, one sees that for the anisotropic conductivity $\tilde{\sigma} = F_*\sigma$ we have

$$K(x, \tilde{\sigma}) = \mu_F(F^{-1}(x)), \quad \text{for } x \in \overline{\mathbb{D}},$$

and hence the maximal anisotropy satisfies $K(\tilde{\sigma}) = \|\mu_F\|_{L^\infty}$.

Let now $\gamma_3 = (F_3)_*\gamma_0$ be an isotropic conductivity in \mathbb{D} and let $\sigma_e = (F_e)_*\gamma_3$ be an anisotropic conductivity in \mathbb{D} . Here, $F_e \circ F_3 \circ f_m|_{\partial\Omega} = f_m$. In particular, the above shows that

$$(f_m)_*\Lambda_\gamma = (f_4 \circ f_3 \circ f_m)_*\Lambda_\gamma = (f_4 \circ f_3)_*\Lambda_{\gamma_0} = (f_4)_*\Lambda_{\gamma_3} = \Lambda_{\sigma_e}.$$

In particular, this implies that inverse problem of finding conductivities σ in \mathbb{D} such that $(f_m)_*\Lambda_\gamma = \Lambda_\sigma$ has a solution $\sigma = \sigma_e$. By Section 2, the knowledge of the boundary $\partial\Omega_m = \partial\mathbb{D}$ and the map $(f_m)_*\Lambda_\gamma$ determines the class $\Sigma(\sigma_e)$ of conductivities in \mathbb{D} . Now we can write the class $\Sigma(\sigma_e)$ also as

$$\Sigma(\sigma_e) = \{F_*\gamma_3 : F : \mathbb{D} \rightarrow \mathbb{D} \text{ is homeomorphism, } F, F^{-1} \in H^1(\Omega; \mathbb{C}), F|_{\partial\mathbb{D}} = f_4\}.$$

Since

$$K(F_*\gamma_3) = \|\mu_F\|_{L^\infty(\mathbb{D})},$$

we see that the conductivity $\sigma_e = (F_e)_*\gamma_3$ corresponding to the extremal map F_e is the unique conductivity σ in the class $\Sigma(\sigma_e)$ that has the smallest possible value of $K(\sigma)$.

Finally, since $|\mu_{F_e}(z)| = c_0$ is constant function of $z \in \mathbb{D}$, and $\sigma_e = (F_e)_*\gamma_3$ with isotropic γ_3 , we see that the ratio of the eigenvalues of the conductivity matrix $\sigma_e(z)$ is constant for $z \in \mathbb{D}$. Thus σ_e has the form $\sigma_e = \hat{\gamma}_{\lambda, \theta, \eta}$ with $c_0 = (1 - \lambda)/(1 + \lambda)$, $\eta = \gamma_3 \circ (F_e)^{-1}$, and some θ . This proves Theorem 1.2. \square

As noted above, the construction of $\hat{\gamma}$ in the above proof did not use the fact that γ is isotropic at all. This shows Remark 1.

Next we proof Proposition 1.3.

Proof. Consider isotropic conductivities γ_1 and γ_2 in Ω . In sequel, we use notation of the proof of Theorem 1.2. By definition, f_m determines a map F_m . The construction of the map F_1 is based on the Beltrami coefficient of the conductivity. Clearly, the Beltrami coefficients for the conductivities $(F_m)_*\gamma_1$ and $(F_m)_*\gamma_2$ coincide, and thus F_1 and Ω_1 can be taken to be the same for both γ_1 and γ_2 . The maps F_2 , F_3 and F_e are constructed by using $\partial\Omega_1$ and F_1 , and thus they coincide for γ_1 and γ_2 . Since in general $\det(F_*\gamma)(x) = \det(\gamma(F^{-1}(x)))$, this proves Proposition 1.3. \square

As noted above, certain assumption on the regularity of the boundary values are necessary, for there are counterexamples to the uniqueness, for example the so-called Strebel's chimney. The current state of the uniqueness question can be found in [5].

We note also that if in formula (3.15) the function ϕ has zeros in Ω , then μ_{F_e} has a singularity of type $\overline{(z - z_0)^j}/(z - z_0)^j$, and this could affect the behaviour of the reconstruction algorithm we propose in a way to explained later. However, in all the numerical examples we have tested these difficulties do not appear, probably since our deformations are relatively small.

4. Electrode model In the numerical simulations below we have used so called complete electrode model [15], which is a certain finite dimensional approximation of Dirichlet-to-Neumann map. This model is chosen as it is an accurate model for the measurements made in practice. As noted before, in experimental measurements one places the measurement electrodes on the boundary, e.g., the skin of the patient, without knowing exact parameterization of the boundary. Thus this model is a paradigm of the case when the boundary is unknown.

To define the electrode model, let $e_j \subset \partial\Omega$, $j = 1, \dots, J$ be disjoint open paths modelling the electrodes that are used for the measurements. Let u solve the equation

$$(4.16) \quad \nabla \cdot \gamma \nabla v = 0 \quad \text{in } \Omega,$$

$$(4.17) \quad z_j \nu \cdot \gamma \nabla v + v|_{e_j} = V_j,$$

$$(4.18) \quad \nu \cdot \gamma \nabla v|_{\partial\Omega \setminus \cup_{j=1}^J e_j} = 0,$$

where V_j are constants representing electric potentials on electrode e_j . This models the case where electrodes e_j having potentials V_j are attached to the boundary, z_j is the contact impedance between electrode e_j and the body surface, and the normal current outside the electrodes vanish. By [15], (4.16-4.18) has a solution $u \in H^1(\Omega)$. The measurements in this model are the currents observed on the electrodes, given by

$$I_j = \frac{1}{|e_j|} \int_{e_j} \nu \cdot \gamma \nabla v(x) ds(x), \quad j = 1, \dots, J.$$

Thus the electrode measurements are given by map $E : \mathbb{R}^J \rightarrow \mathbb{R}^J$, $E(V_1, \dots, V_J) = (I_1, \dots, I_J)$. We say that E is the electrode measurement matrix for $(\partial\Omega, \gamma, e_1, \dots, e_J, z_1, \dots, z_J)$. Let Ω and $\tilde{\Omega}$ be $C^{1,\alpha}$ -smooth domains. We say that $f : \partial\Omega \rightarrow \partial\tilde{\Omega}$ is length preserving on $\cup_{j=1}^J e_j$ if $\|Df(\tau)\| = 1$ for $x \in \cup_{j=1}^J e_j$ where τ is the unit tangent vector of $\partial\Omega$.

PROPOSITION 4.1. Let Ω and $\tilde{\Omega}$ be $C^{1,\alpha}$ -smooth domains and $F : \bar{\Omega} \rightarrow \bar{\tilde{\Omega}}$ be a $C^{1,\alpha}$ -diffeomorphism, $e_j \subset \partial\Omega$ be disjoint open sets, and γ be a conductivity on Ω . Let $f = F|_{\partial\Omega}$, $\tilde{e}_j = f(e_j) \subset \partial\tilde{\Omega}$ and $\tilde{\gamma} = (F)_*\gamma$. Assume that f is length preserving on $\cup_{j=1}^J e_j$. Then the electrode measurement matrices E for $(\partial\Omega, \gamma, e_1, \dots, e_J, z_1, \dots, z_J)$ and \tilde{E} for $(\partial\tilde{\Omega}, \tilde{\gamma}, \tilde{e}_1, \dots, \tilde{e}_J, z_1, \dots, z_J)$ coincide.

Proof. We start with an invariant formulation of electrode measurements E . For this, let R be the Robin-to-Neumann map given by $Rf = \nu \cdot \gamma \nabla u|_{\partial\Omega}$ where u is solution of

$$(4.19) \quad \begin{aligned} \nabla \cdot \gamma \nabla u &= 0 \quad \text{in } \Omega \\ z\nu \cdot \gamma \nabla u + \eta u &= h, \end{aligned}$$

where $z = z(x)$ is $C^\infty(\partial\Omega)$ function such that $z|_{e_j} = z_j$ and $\eta = \sum_{j=1}^J \chi_{e_j}(x)$, where χ_{e_j} is the characteristic function of electrode e_j . Note that if the boundary and the contact impedance are known, the Robin-to-Neumann and the Dirichlet-to-Neumann maps determine each other, that is, they represent equivalent information.

Consider now the bilinear form corresponding to linear maps $E : \mathbb{R}^J \times \mathbb{R}^J \rightarrow \mathbb{R}$ and $R : H^{-1/2}(\partial\Omega) \times H^{-1/2}(\partial\Omega) \rightarrow \mathbb{R}$ given by

$$E[V, \tilde{V}] = \sum_{j=1}^J (EV)_j \tilde{V}_j|_{e_j}, \quad R[h, \tilde{h}] = \int_{\partial\Omega} (Rh) \tilde{h} ds.$$

Let $S = \text{span}(\chi_{e_j} : j = 1, \dots, J) \subset H^{-1/2}(\partial\Omega)$ and define $M : V = (V_j)_{j=1}^J \mapsto \sum_{j=1}^J V_j \chi_{e_j}$ to be a map $M : \mathbb{R}^J \rightarrow S$. Then

$$(4.20) \quad E[V, \tilde{V}] = R[MV, M\tilde{V}].$$

Moreover, for $h = MV$ with some $V \in \mathbb{R}^J$, we have

$$(4.21) \quad R[h, h] = \int_{\partial\Omega} (u + z\nu \cdot \gamma \nabla u) \nu \cdot \gamma \nabla u ds = \int_{\Omega} \gamma \nabla u \cdot \nabla u dx + \int_{\partial\Omega} z |\nu \cdot \gamma \nabla u|^2 ds$$

where u solves (4.19). Above the integral over Ω is invariant in coordinate deformations. Note that in the above formula the integral over the boundary is not coordinate invariant.

Let \tilde{E} be electrode measurement matrix for $\tilde{\gamma}$ in $\tilde{\Omega}$ with electrodes $\tilde{e}_j = f(e_j)$ and let \tilde{R} be the Robin-to-Neumann map for $\tilde{\gamma}$ defined analogously to (4.19). Since f is length preserving on the electrodes, we see using (1.3) that $\nu \cdot \gamma \nabla u(x) = \nu \cdot \tilde{\gamma} \nabla \tilde{u}(f(x))$, for $\tilde{u} = u \circ F^{-1}$ and $x \in \partial\Omega$, and thus we can see from (4.21) that

$$R[h, \tilde{h}] = \tilde{R}[h \circ f^{-1}, \tilde{h} \circ f^{-1}],$$

for $h, \tilde{h} \in H^{-1/2}(\partial\Omega)$ supported in the closure of $\cup_{j=1}^J e_j$. Thus for the map $\tilde{M} : V \mapsto \sum_{j=1}^J V_j \chi_{\tilde{e}_j}$ we have by formula (4.20) that $\tilde{E}[V, \tilde{V}] = \tilde{R}[\tilde{M}V, \tilde{M}\tilde{V}]$. Combining this and (4.20) we obtain

$$E[V, V'] = \tilde{E}[V, V'].$$

In particular, this implies that the matrices E and \tilde{E} coincide. \square

In particular, in the case where $\tilde{\Omega}$ is the model domain Ω_m and $f = f_m : \partial\Omega \rightarrow \partial\Omega_m$ is the model map for the boundary, the assumption that f is length preserving on electrodes means the very natural assumption that in electrode measurements the parametrization of electrodes are known. Then by Proposition 4.1, the electrode model discretization E of Λ_γ equals the corresponding discretization \tilde{E} of $(f_m)_*\Lambda_\gamma$. Summarizing, the electrode measurements does not change if we have modeled the geometry of the boundary incorrectly but the electrodes are modeled correctly.

5. Numerical examples The performance of the proposed method is evaluated by test cases with simulated EIT data. First, in Section 5.1 we briefly discuss the discretization and the computational methods that are used, and the results are then given in Section 5.2.

5.1. Discretization and notation The numerical solution of the forward model is based on the finite element method (FEM). The variational formulation and the finite element discretization of the electrode model (4.16-4.18) in the case of isotropic conductivities have been previously discussed e.g. in [10]. The extension of the FEM-model to the anisotropic case is straightforward, the details will be given in a subsequent publication.

For the functions $\eta(x)$ and $\theta(x)$ in equation (1.5) we use piecewise constant approximations that are defined on a lattice of regular pixels. Thus, we have

$$(5.22) \quad \eta = \sum_{i=1}^M \eta_i \chi_i(x), \quad \theta = \sum_{i=1}^M \theta_i \chi_i(x)$$

where χ_i is the characteristic function of the i^{th} pixel in the lattice. Within the discretization (5.22), the parameters η and θ are identified with the coefficient vectors

$$\begin{aligned} \eta &= (\eta_1, \eta_2, \dots, \eta_M)^T \in \mathbb{R}^M \\ \theta &= (\theta_1, \theta_2, \dots, \theta_M)^T \in \mathbb{R}^M \end{aligned}$$

and λ is a scalar parameter. Note that as $\hat{\gamma}_{\lambda, \eta, \theta} = \hat{\gamma}_{\lambda', \eta, \theta'}$, where $\lambda' = 1/\lambda$ and $\theta'(x) = \theta(x) + \pi/2$, we can assume in looking the minimizing uniformly anisotropic conductivity that λ gets values $\lambda > 0$.

In practical EIT devices, the measurements are made such that known currents are injected into the domain Ω through some of the the electrodes at $\partial\Omega$, and the corresponding voltages needed to maintain these currents are measured on some of electrodes. Often, voltages are measured only on those electrodes that are not used to inject current. Thus, measurements made give only partial information on the matrix E . To take this in to account, we introduce the following notation for the discretized problem. We assume that the EIT experiment consists of a set of K partial voltage measurements, $V^{(j)}$, $j = 1, \dots, K$. For each measurement, consider a current pattern $I^{(j)}$, $j = 1, \dots, K$ such that $\sum_{\ell=1}^J I_\ell^{(j)} = 0$. Typically, the corresponding measurements are the voltages (potential differences) between pairs of neighboring electrodes. Let us assume that the measurement vector $V^{(j)}$ corresponding to the current pattern $I^{(j)}$ consist of L voltage measurements,

i.e., we have $V^{(j)} \in \mathbb{R}^L$. Thus, we write $V^{(j)} = P_j E^{-1} I^{(j)} + \epsilon^{(j)}$, where E is the electrode measurement matrix, random vector $\epsilon^{(j)}$ models the observation errors and $P_j : \mathbb{R}^J \rightarrow \mathbb{R}^L$ is a measurement operator that maps the electrode potentials to measured voltages.

In the inverse problem, the voltage measurements $V^{(1)}, V^{(2)}, \dots, V^{(K)}$ are concatenated into a single vector

$$V = (V^{(1)}, V^{(2)}, \dots, V^{(K)})^T \in \mathbb{R}^N, \quad N = KL.$$

For the finite element based discretization of the forward problem $U : \mathbb{R}^{2M+1} \mapsto \mathbb{R}^N$, we use the notation

$$U(\eta, \theta, \lambda) = (U^{(1)}(\eta, \theta, \lambda), U^{(2)}(\eta, \theta, \lambda), \dots, U^{(K)}(\eta, \theta, \lambda))^T \in \mathbb{R}^N,$$

respectively. Here, $U^{(j)}(\eta, \theta, \lambda) = P_j E^{-1}(\eta, \theta, \lambda) I^{(j)} \in \mathbb{R}^L$ corresponds to partial voltage measurement with current pattern $I^{(j)}$ and conductivity $\hat{\gamma}_{\eta, \theta, \lambda}$.

Using the above notations, we write the discretized and regularized version of our inverse problem as finding minimizer of the functional

$$(5.23) \quad F(\eta, \theta, \lambda) = \|V - U(\eta, \theta, \lambda)\|^2 + W_\eta(\eta) + W_\theta(\theta) + W_\lambda(\lambda), \quad \eta > 0, \lambda > 0,$$

where the regularizing penalty functionals are of the form

$$(5.24) \quad W_\eta(\eta) = \alpha_0 \sum_{i=1}^M \eta_i^2 + \alpha_1 \sum_{i=1}^M \sum_{j \in \mathcal{N}_i} |\eta_i - \eta_j|^2,$$

$$(5.25) \quad W_\theta(\theta) = \beta_0 \sum_{i=1}^M \theta_i^2 + \beta_1 \sum_{i=1}^M \sum_{j \in \mathcal{N}_i} |e^{i\theta_i} - e^{i\theta_j}|^2,$$

$$(5.26) \quad W_\lambda(\lambda) = \beta_2 (\log(\lambda) + \nu^{-2} \log(\lambda)^2)$$

and \mathcal{N}_i denotes the usual 4-point nearest neighborhood system for pixel i in the lattice.

Our objective is to minimize the functional (5.23) by gradient based optimization methods. Here we face the difficulty due to the positivity constraints. To take the positivity constraint into account we employ the interior point search method [7]. In the interior point search the original constrained problem (5.23) is replaced by a sequence of augmented unconstrained problems of the form

$$(5.27) \quad \tilde{F}_j(\eta, \theta, \lambda) = F(\eta, \theta, \lambda) + W_+^{(j)}(\eta)$$

where $W_+^{(j)}(\eta)$ is a penalty functional of the form

$$(5.28) \quad W_+^{(j)}(\eta) = \xi_j \sum_{i=1}^M \frac{1}{\eta_i}$$

and $\{\xi_j\}$ is a sequence of decreasing positive parameters such that $\xi_j \rightarrow 0$ as $j \rightarrow \infty$. Using a suitably chosen sequence of penalty functionals $W_+^{(j)}$, the solutions of the unconstrained problems converge (asymptotically) to the solution of the original constrained problem. The positivity constraint for λ can be taken care with similar techniques. However, it is our experience that the positivity constraint was not needed for λ .

For the minimization of the functionals (5.27) we employ the Gauss-Newton optimization method with an explicit line search algorithm.

5.2. *Results* In this section, we evaluate the performance of the proposed method with three different test cases. The first test case is EIT data from an ellipse domain Ω , in the second test case we consider an ellipse domain with a sharp cut and in the last test case the domain is a smooth Fourier domain which has some resemblance with the cross section of the human body. In all of these cases, we use the unit disk as the model domain Ω_m .

In the simulations, we assume an EIT system with $J = 16$ electrodes. In each of the test cases, the electrodes were located at approximately equally spaced positions at the exterior boundary $\partial\Omega$ of the target domain Ω . The size of the electrodes were chosen such that the electrodes covered approximately 50% of the boundary $\partial\Omega$.

The EIT measurements were simulated using the usual adjacent pair drive data acquisition method. In the adjacent drive method, currents $+1$ and -1 are injected through two neighboring electrodes, say electrodes e_n and e_{n+1} , and current through other electrodes is zero. The voltages are measured between all J pairs of neighboring electrodes. However, three of these measurements are typically neglected since they include either one or both of the current feeding electrodes e_n or e_{n+1} . The rationale behind this is that the electrode contact impedances z_j are usually not known accurately. The possible errors in the contact impedance values cause a systematic error between the measured voltage and the forward model for the measurement made on the current feeding electrodes, and this error causes artefacts to the numerical reconstruction, see e.g. [9]. Thus, with the adjacent pair drive method each partial measurement consist of $L = J - 3$ voltage measurements and we have $V^{(j)} \in \mathbb{R}^{J-3}$. This data acquisition process is then repeated for all the J pairs of adjacent electrodes, leading to total of $N = J(J - 3)$ voltage measurements for one EIT experiment. Thus, with the $J = 16$ electrode system we have $V \in \mathbb{R}^{208}$.

The simulated EIT measurements were computed using the isotropic EIT model and the finite element method. To simulate measurement noise, we added Gaussian random noise with standard deviation of 1% of the maximum value of the simulated voltages to the data. In all of the following test cases we used value $z_\ell = 1$ for the electrode contact impedances. These were assumed known in the inverse problem.

The results for the first test case are shown in Figures 1-2. The target conductivity is shown in the top left image in Figure 1. The target domain Ω is an ellipse with main axes 1.25 in the horizontal direction and 0.8 in the vertical direction. For the simulation of the EIT measurements, the domain was discretized into a finite element mesh that consisted of 1256 nodal points and 2350 triangular elements.

The reconstruction of the conductivity γ with isotropic EIT model in the correct domain Ω is shown in the top right image in Figure 1. The reconstruction was obtained by using similar optimization techniques that are explained in the previous section. However, in the case of isotropic model the unknown parameter vector is the conductivity vector $\gamma \in \mathbb{R}^M$ and the optimization functionals for the interior point search can be written as

$$(5.29) \quad H_j(\gamma) = \|V - U(\gamma)\|^2 + W_\gamma(\gamma) + W_+^{(j)}(\gamma),$$

where $U(\gamma)$ denotes the forward problem for the isotropic model, $W_\gamma(\gamma)$ and $W_+^{(j)}(\gamma)$ are defined by equations (5.24) and (5.28), respectively. To compute the reconstruction in the top right image in Figure 1, the domain Ω was triangulated to a finite element mesh that consisted of 2326 elements with 1244 nodal points. The conductivity was represented in a lattice of $M = 451$ pixels (i.e., $\gamma \in \mathbb{R}^{451}$). The regularization parameters for the penalty

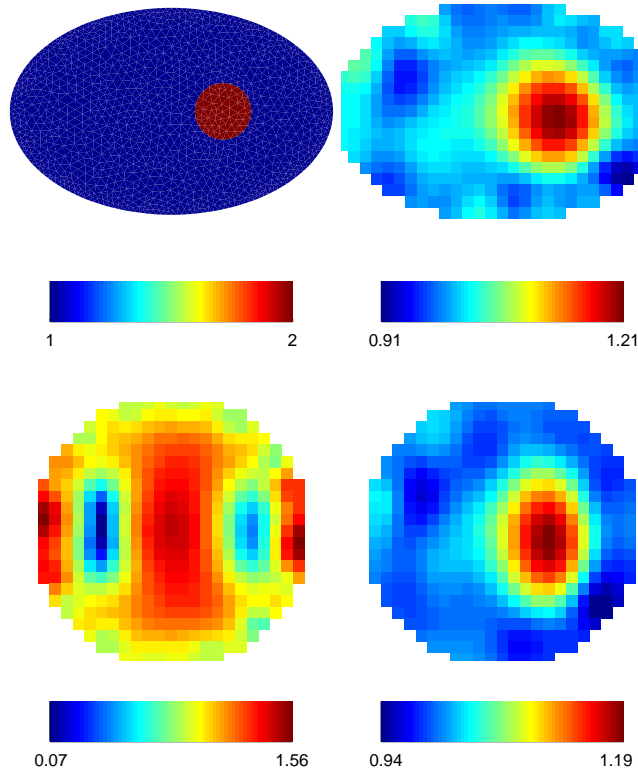


Figure 1: Test case with EIT data from an ellipse domain Ω . The main axes of the ellipse were 1.25 in horizontal direction and 0.8 in the vertical direction. Top left: Simulated conductivity distribution γ . Top right: Reconstruction of γ with isotropic EIT model in the correct domain Ω . Bottom left: Reconstruction of γ with isotropic model in incorrectly modeled geometry. The reconstruction domain Ω_m was the unit disk. Bottom right: Reconstruction of η with the uniformly anisotropic model in the same unit disk geometry.

functional $W_\gamma(\gamma)$ in equation (5.29) were $\alpha_0 = 10^{-8}$ and $\alpha_1 = 10^{-4}$. When computing the reconstruction in the correctly modeled geometry, the interior point search was kept inactive (i.e., the sequence $\{\xi_j\}$ of interior point search parameters were all zeros). The conductivity vector was initialized to constant value of one in the optimization process. The Gauss-Newton optimization algorithm was iterated until convergence was obtained.

The image in the bottom left in Figure 1 shows the reconstruction of the conductivity with the isotropic model in incorrectly modeled geometry Ω_m . In this case, the computational domain Ω_m was the unit disk which was triangulated to 2190 elements with 1176 nodal points. The conductivity parameters were represented in a lattice of $M = 437$ pixels (i.e., $\gamma \in \mathbb{R}^{437}$). The regularization parameters for the penalty functional $W_\gamma(\gamma)$ in equation (5.29) were $\alpha_0 = 10^{-8}$ and $\alpha_1 = 2 \cdot 10^{-4}$. The sequence of interior point search parameters $\{\xi_j\}$ were from $2 \cdot 10^{-5}$ to $5 \cdot 10^{-6}$. The constant vector $\gamma = 1 \in \mathbb{R}^{437}$ was used as the initial guess in the Gauss-Newton optimization.

The image in the bottom right in Figure 1 shows the reconstruction of η with the uniformly anisotropic model in incorrectly modeled geometry Ω_m . Here, by the solution

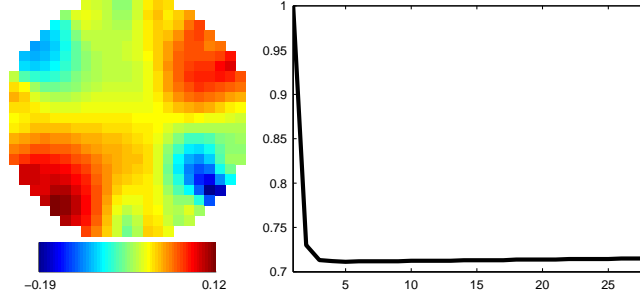


Figure 2: Test case with EIT data from an ellipse domain Ω . The main axes of the ellipse were 1.25 in horizontal direction and 0.8 in the vertical direction. Left: Reconstruction of the anisotropy angle parameter θ in the incorrectly modeled geometry. The computational domain Ω_m was the unit disk. Right: Evolution of the anisotropy parameter λ during the Gauss-Newton iteration.

in the *uniformly anisotropic model* we mean the optimal solution of the form (1.5) of the minimization problem. The reconstruction was obtained by minimizing sequence of optimization functionals of the form (5.27). The reconstructed angle parameter θ is shown in the left image in Figure 2, and the evolution of the parameter λ during the iteration is shown in the right image in Figure 2. The computational domain Ω_m was the unit disk. The finite element triangularization and the amount of the image pixels were the same as in the isotropic case in bottom left image in Figure 1. Thus, the unknowns in the inverse problem are $\eta \in \mathbb{R}^{437}$, $\theta \in \mathbb{R}^{437}$ and $\lambda \in \mathbb{R}$. The parameters for the regularizing penalty functionals $W_\eta(\eta)$ in equation (5.24) were $\alpha_0 = 10^{-8}$ and $\alpha_1 = 10^{-4}$. The parameters for the penalty functionals $W_\theta(\theta)$ and $W_\lambda(\lambda)$ in equations (5.25-5.26) were $\beta_0 = 10^{-8}$, $\beta_1 = 5 \cdot 10^{-6}$ and $\beta_2 = 0$, respectively. The sequence of interior point search parameters $\{\xi_j\}$ was from $1 \cdot 10^{-5}$ to $1 \cdot 10^{-12}$. The Gauss-Newton optimization was started from the constant values $\eta = 1 \in \mathbb{R}^{437}$, $\theta = 0 \in \mathbb{R}^{437}$ and $\lambda = 1$ which correspond to isotropic unit conductivity.

The results for the second test case are shown in Figure 3. The simulated conductivity distribution is shown in the top left image. In this case the domain Ω is a truncated ellipse with main axes 1.1 in the horizontal direction and 0.9 in the vertical direction, respectively. For the simulation of the EIT measurements, the domain was divided to a finite element mesh of 2383 triangular elements with 1240 nodes.

The top right image in Figure 3 shows the reconstruction of the conductivity with the isotropic model in the correct geometry. For the reconstruction, the domain Ω was divided to a finite element mesh of 2337 triangular elements with 1217 nodes and the conductivity was represented on a lattice of $M = 455$ pixels. Thus, the unknown parameter vector was $\gamma \in \mathbb{R}^{455}$. The regularization parameters for the penalty functional $W_\gamma(\gamma)$ in equation (5.29) were $\alpha_0 = 10^{-8}$ and $\alpha_1 = 10^{-4}$. The sequence of interior point search parameters $\{\xi_j\}$ was all zeros. The Gauss-Newton optimization was started from the constant unit conductivity.

The bottom left image in Figure 3 shows the reconstructed conductivity with the isotropic model in the incorrectly modeled geometry. The reconstruction domain Ω_m was the unit disk. The finite element mesh and pixel lattice were the same that were used for the unit disk in Figure 1. Thus, the unknown conductivity vector was $\gamma \in \mathbb{R}^{437}$. The

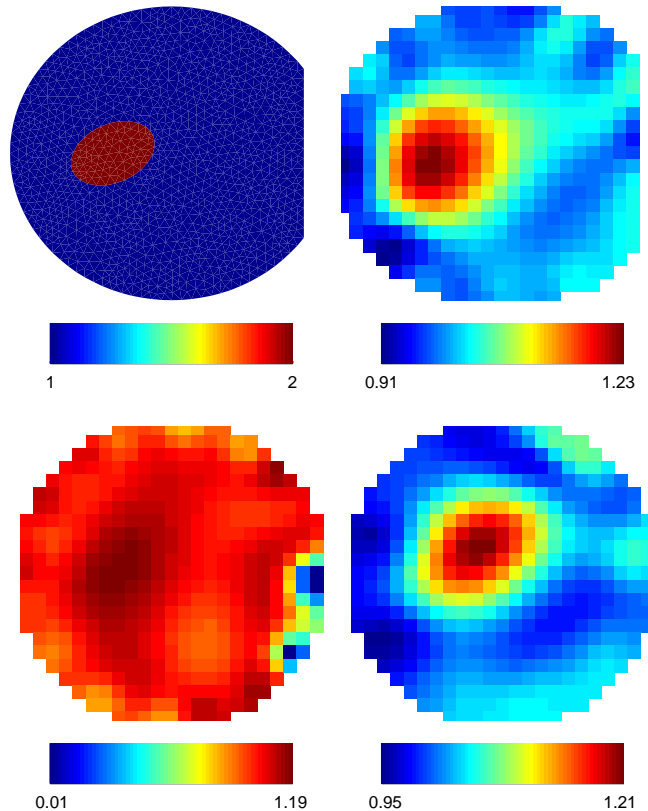


Figure 3: Test case with EIT data from a truncated ellipse domain Ω with main axes $a = 1.1$ and $b = 0.9$. Top left: Simulated conductivity distribution γ . Top right: Reconstruction of the conductivity γ with isotropic model in the correct geometry Ω . Bottom left: Reconstruction of γ with the isotropic model in incorrectly modeled geometry. The reconstruction domain Ω_m was the unit disk. Bottom right: Reconstruction of the parameter η with the uniformly anisotropic model in the same unit disk geometry.

parameters for the regularizing penalty functional $W_\gamma(\gamma)$ were $\alpha_0 = 10^{-8}$ and $\alpha_1 = 10^{-4}$, and the sequence of interior point search parameters $\{\xi_j\}$ was from 10^{-5} to 10^{-8} . The constant unit conductivity was used as the initial guess in the optimization.

The bottom right image in Figure 3 shows the reconstruction of η with the uniformly anisotropic model in the incorrectly modeled geometry. The computational domain Ω_m was the unit disk with the same discretization that was used in Fig. 1. Thus, the unknowns were $\eta \in \mathbb{R}^{437}$, $\theta \in \mathbb{R}^{437}$ and $\lambda \in \mathbb{R}$. The parameters for the regularizing penalty functionals $W_\eta(\eta)$ in equation (5.24) were $\alpha_0 = 10^{-8}$ and $\alpha_1 = 10^{-4}$. The parameters for the penalty functionals $W_\theta(\theta)$ and $W_\lambda(\lambda)$ in equations (5.25-5.26) were $\beta_0 = 10^{-8}$, $\beta_1 = 5 \cdot 10^{-6}$ and $\beta_2 = 0$, respectively. The sequence of parameters $\{\xi_j\}$ was from 10^{-5} to 10^{-12} . The initializations for the parameters in the Gauss-Newton optimization were the constant values $\eta = 1 \in \mathbb{R}^{437}$, $\theta = 0 \in \mathbb{R}^{437}$ and $\lambda = 1$.

The results for the last test case are shown in Figure 4. In this case, the target domain Ω is bounded by a smooth Fourier boundary $\partial\Omega$. The true isotropic conductivity distribution within the domain Ω is shown in the top left image in Figure 4. For the simulation of the

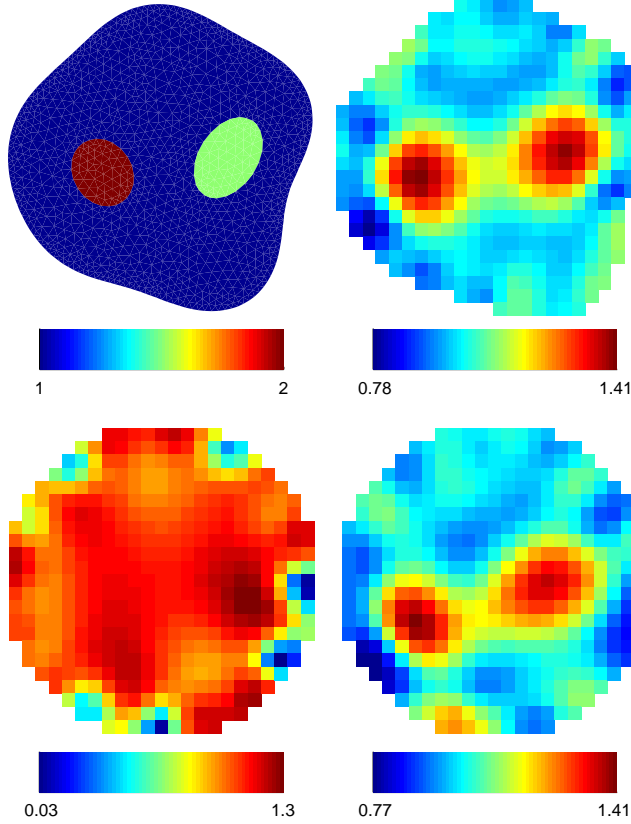


Figure 4: Test case with EIT data from an arbitrary domain Ω . Top left: True conductivity distribution γ . Top right: Reconstruction of the conductivity γ with isotropic model in the correct geometry Ω . Bottom left: Reconstruction of γ with the isotropic model in incorrectly modeled geometry. The reconstruction domain Ω_m was the unit disk. Bottom right: Reconstruction of the parameter η with the uniformly anisotropic model in the same unit disk geometry.

EIT measurements, the domain Ω was divided to a mesh of 2316 triangular elements with 1239 nodes.

The reconstruction of the conductivity γ with the isotropic model in the correct geometry Ω is shown in the top right image in Figure 4. The domain was divided to a mesh of 2200 triangular elements with 1181 nodes for the image reconstruction process. The number of pixels was $M = 446$ for the representation of the conductivity image (i.e. $\gamma \in \mathbb{R}^{446}$). The regularization parameters for the penalty functional $W_\gamma(\gamma)$ were $\alpha_0 = 10^{-8}$ and $\alpha_1 = 10^{-5}$ and the sequence of parameters $\{\xi_j\}$ was all zeros. The constant unit conductivity was used as the initial guess in the Gauss-Newton optimization algorithm.

The reconstruction of the conductivity γ with the isotropic model in the incorrectly modeled geometry is shown in the bottom left image in Figure 4. The reconstruction domain Ω_m was the unit disk. The finite element mesh and the pixel lattice were the same that were used in Figures 1-3. Thus, the parameter vector in the inverse problem was $\gamma \in \mathbb{R}^{437}$. The parameters in the penalty functional $W_\gamma(\gamma)$ were $\alpha_0 = 10^{-8}$ and $\alpha_1 = 2 \cdot 10^{-4}$, and the sequence of parameters $\{\xi_j\}$ was from $2 \cdot 10^{-5}$ to $5 \cdot 10^{-6}$. The

constant unit conductivity was used as the initial guess in the optimization.

The reconstruction of η with the uniformly anisotropic model in the incorrectly modeled geometry is shown in the bottom right image in Figure 4. The reconstruction domain Ω_m was the unit disk with the same discretization as in Figures. 1-3. Thus, the unknown parameter vectors were $\eta \in \mathbb{R}^{437}$, $\theta \in \mathbb{R}^{437}$ and $\lambda \in \mathbb{R}$. The parameters for the regularizing penalty functionals $W_\eta(\eta)$ in equation (5.24) were $\alpha_0 = 10^{-8}$ and $\alpha_1 = 10^{-5}$. The parameters for the penalty functionals $W_\theta(\theta)$ and $W_\lambda(\lambda)$ in equations (5.25-5.26) were $\beta_0 = 10^{-8}$, $\beta_1 = 5 \cdot 10^{-6}$ and $\beta_2 = 0$, respectively. The sequence of parameters $\{\xi_j\}$ was from 10^{-5} to 10^{-12} . The initializations for the image parameters were the constant values $\eta = 1 \in \mathbb{R}^{437}$, $\theta = 0 \in \mathbb{R}^{437}$ and $\lambda = 1$.

6. Discussion As can be seen from Figures 1-4, the proposed approach gives good results. In all test cases, the traditional reconstructions with the isotropic model are erroneous when the imaging geometry is modeled incorrectly. The effects of erroneous geometry are seen in the reconstructions as distortions and severe artefacts, especially near the boundary. On the other hand, the reconstructions of η with the uniformly anisotropic model in the same erroneous geometry are clear of these artefacts and represent a deformed picture of the original isotropic conductivity. These results indicate that the proposed method offers an efficient tool to eliminate the difficulties that arise from inaccurately known geometry in practical EIT experiments.

Acknowledgements The authors are thankful for prof. Kari Astala and prof. Seppo Rickman for discussions on quasiconformal maps that were crucial for obtained results. This work was supported by the Academy of Finland (projects 203985, 72434, and 102175).

References

- [1] Adler A, Guardo R, and Berthiaume Y. Impedance imaging of lung ventilation: Do we need to account for chest expansion? *IEEE Trans. Biomedical Engineering*, 43 (1996), 414–420.
- [2] Ahlfors, L.V. *Lectures on quasiconformal maps*, Van Nostrand (1966)
- [3] Astala, K., Lassas M., and Päivärinta L. Calderón’s inverse problem for anisotropic conductivity in plane, preprint <http://arxiv.org/abs/math.AP/0401410>
- [4] Astala, K. and Päivärinta L. Calderon’s inverse conductivity problem in the plane, Preprint, *Reports of the department of mathematics, University of Helsinki* (370), 2003.
- [5] Bozin, V., Lakic N., Markovic V., and Mateljevic M. Unique extremality, *J.Anal.Math.* 75 (1998), 299–338
- [6] Calderón, A-P. On an inverse boundary value problem, Seminar on Numerical Analysis and its Applications to Continuum Physics (Rio de Janeiro, 1980), *Soc. Brasil Mat.* (1980), 65–73, Rio de Janeiro
- [7] Fiacco A. and McCormick G. *Nonlinear programming: sequential unconstrained minimization techniques*. Classics in Applied Mathematics, 4. SIAM, Philadelphia, 1990. xvi+210 pp

- [8] Gersing E, Hoffman B, and Osypka M. Influence of changing peripheral geometry on electrical impedance tomography measurements. *Medical & Biological Engineering & Computing*,34 (1996), 359–361.
- [9] Kolehmainen V, Vauhkonen M, Karjalainen P.A , and Kaipio J.P. Assessment of errors in static electrical impedance tomography with adjacent and trigonometric current patterns. *Physiological Measurement*, 18(1997), 289–303.
- [10] Kaipio J., Kolehmainen V., Somersalo E., and Vauhkonen M. Statistical inversion and Monte Carlo sampling methods in electrical impedance tomography. *Inverse Problems*, 16(2000), 1487–1522.
- [11] Lehto, O. *Univalent functions and Teichmüller mappings*, Graduate texts in mathematics 109, Springer 1986.
- [12] Nachman, A. Reconstructions from boundary measurements, *Ann. Math.* 128 (1988), 531–576.
- [13] Nachman, A. Global uniqueness for a two–dimensional inverse boundary value problem, *Ann. Math.* 143 (1996), 71–96.
- [14] Pommerenke, Ch. *Boundary behaviour of conformal maps*. Grundlehren der Mathematischen Wissenschaften, 299. Springer-Verlag, Berlin, 1992. x+300 pp.
- [15] Somersalo E., Cheney M., and Isaacson D. Existence and uniqueness for electrode models for electric current computed tomography. *SIAM J. Appl. Math.*, 52(1992), 1023–1040.
- [16] Strebel. K. On the existence of extremal Teichmüller mappings, *J. Analyse Math.* 30 (1976), 464–480.
- [17] Sylvester, J. An anisotropic inverse boundary value problem, *Comm. Pure Appl. Math.* 43 (1990), 201–232.
- [18] Sylvester, J. and Uhlmann G. A global uniqueness theorem for an inverse boundary value problem, *Ann. of Math.* 125 (1987), 153–169.